# The Location of Young Pulsar PSR J0837–2454: Galactic Halo or Local Supernova Remnant?

Nihan Pol[1,2,3], Sarah Burke-Spolaor[1,2,4], Natasha Hurley-Walker[5], Harsha Blumer[1,2], Simon Johnston[6], Michael Keith[7], Evan F. Keane[8], Marta Burgay[9], Andrea Possenti[9,10], Emily Petroff[11], and N. D. Ramesh Bhat[5]

[1] Department of Physics and Astronomy, West Virginia University, Morgantown, West Virginia 26506, USA
[2] Center for Gravitational Waves and Cosmology, West Virginia University, Chestnut Ridge Research Building, Morgantown, WV 26505, USA
[3] Department of Physics and Astronomy, Vanderbilt University, 2301 Vanderbilt Place, Nashville, TN 37235, USA
[4] CIFAR Azrieli Global Scholar, Canadian Institute for Advanced Research, MaRS Centre West Tower, 661 University Avenue, Suite 505, Toronto ON M5G 1M1, Canada
[5] International Centre for Radio Astronomy Research, Curtin University, Bentley, WA 6102, Australia
[6] CSIRO Astronomy and Space Science, Australia Telescope National Facility, PO Box 76, Epping, NSW 1710, Australia
[7] Jodrell Bank Centre for Astrophysics, University of Manchester, Alan Turing Building, Oxford Road, Manchester M13 9PL, UK
[8] Centre for Astronomy, School of Physics, National University of Ireland Galway, University Road, Galway, H91 TK33, Ireland
[9] INAF—Osservatorio Astronomico di Cagliari, via della Scienza 5, I-09047 Selargius (CA), Italy
[10] University of Cagliari, Department of Physics, S.P. Monserrato-Sestu Km I-0,700-09042 Monserrato (CA), Italy
[11] Anton Pannekoek Institute for Astronomy, University of Amsterdam, Science Park 904, 1098 XH Amsterdam, The Netherlands

## Abstract

We present the discovery and timing of the young (age $\sim$28.6 kyr) pulsar PSR J0837–2454. Based on its high latitude ($b = 9°.8$) and dispersion measure (DM = 143 pc cm$^{-3}$), the pulsar appears to be at a $z$-height of >1 kpc above the Galactic plane, but near the edge of our Galaxy. This is many times the observed scale height of the canonical pulsar population, which suggests this pulsar may have been born far out of the plane. If accurate, the young age and high $z$-height imply that this is the first pulsar known to be born from a runaway O/B star. In follow-up imaging with the Australia Telescope Compact Array (ATCA), we detect the pulsar with a flux density $S_{1400} = 0.18 \pm 0.05$ mJy. We do not detect an obvious supernova remnant around the pulsar in our ATCA data, but we detect a colocated, low-surface-brightness region of $\sim$1°.5 extent in archival Galactic and Extragalactic All-sky MWA Survey data. We also detect colocated H$\alpha$ emission from the Southern H$\alpha$ Sky Survey Atlas. Distance estimates based on these two detections come out to $\sim$0.9 kpc and $\sim$0.2 kpc, respectively, both of which are much smaller than the distance predicted by the NE2001 model (6.3 kpc) and YMW model (>25 kpc) and place the pulsar much closer to the plane of the Galaxy. If the pulsar/remnant association holds, this result also highlights the inherent difficulty in the classification of transients as "Galactic" (pulsar) or "extragalactic" (fast radio burst) toward the Galactic anticenter based solely on the modeled Galactic electron contribution to a detection.

*Unified Astronomy Thesaurus concepts:* pulsars (1306); radio pulsars (1353); Supernova remnants (1667)

## 1. Introduction

Pulsars form in supernovae (SNe), resulting from the core collapse of massive stars. This explosion creates a supernova remnant (SNR), which, if not too distant, can be detectable for thousands of years. This evolutionary association of pulsars in supernova births leads to two clear observational effects: first, both SNR and young pulsars are observed at low Galactic latitudes $\lesssim$300 pc, where the bulk of O/B-type stars reside (Maíz-Apellániz 2001); and second, we find that many young pulsars are associated with an SNR; this appears to be the case for pulsars with ages of up to a few tens of kyr (Wolszczan et al. 1991; Frail et al. 1994; Kaspi et al. 2001; Camilo et al. 2006, 2002).

SNRs are excellent tools for probing various properties of the interstellar medium and the pulsar itself. The presence of an SNR can provide information about the local electron density (e.g., Frail et al. 1996) and magnetic field strength of the pulsar (e.g., Brazier & Johnston 1999). The size of the SNR along with measurement of its expansion velocity can provide an estimate of the age of the pulsar. The relative position of the pulsar with respect to the SNR can be used to infer the velocity of the pulsar, and thus, provide estimates on the kick received by the pulsar at the time of the SN explosion (Migliazzo et al. 2002).

In this publication, we report the discovery, timing, and follow-up of a pulsar that appears, based on the distance derived from its dispersion measure (DM), to lie at least 1 kpc above the outer arms of the Galaxy. Based on the current period, $P$, and period derivative, $\dot{P}$, of the pulsar, this pulsar appears to be young, with its characteristic age given by Lorimer & Kramer (2012)

$$\tau_c = \frac{P}{(n-1)\dot{P}}\left[1 - \left(\frac{P_{\text{birth}}}{P}\right)^{n-1}\right], \tag{1}$$

where $n$ is the braking index of the pulsar and $P_{\text{birth}}$ is the spin period of the pulsar when it was born. Given the large period of PSR J0837–2454 ($P = 629.4102$ ms), we can safely assume that $P_{\text{birth}} \ll P$. Assuming that the pulsar spin-down is from magnetic-dipole braking only, the braking index is $n = 3$, and Equation (1) reduces to

$$\tau_c = \frac{P}{2\dot{P}} \approx 28.6 \text{ kyr.} \tag{2}$$

The young age and high Galactic latitude of this pulsar are contrary to the standard formation scenario described above. The location of this pulsar can be explained via two different scenarios: (i) it was born at this high Galactic latitude by a runaway O/B star; or (ii) it was born closer to the plane of the

Galaxy and the distance derived using the NE2001 model (Cordes & Lazio 2002) is incorrect.

The presence of a supernova remnant around the pulsar would allow us to independently estimate the distance to the pulsar–SNR system using the Sigma-D relation (Green 1984). In addition, there are only six confirmed Galactic supernovae that are above a Galactic latitude of $b \gtrsim 8.5$ (Green 2019), while only two of these have a neutron star at their center (Gotthelf & Halpern 2007; Abdo et al. 2008). However, both of these neutron stars are radio-silent, and thus, a supernova remnant detection around this pulsar would be a valuable addition to this sample. Assuming the characteristic age is a reasonable assumption of the true age of the pulsar and SNR, we would expect the SNR to be in its late Sedov (Sedov 1959) or early radiative evolution phase (Cioffi et al. 1988) and thus would see synchrotron emission at radio wavelengths from the SNR, with the possibility of further emission at X-ray wavelengths (Alsabti & Murdin 2017).

If the pulsar is indeed as high as the DM-derived distance, that would imply that the progenitor of this pulsar was likely a runaway O/B star. Runaway stars (Humason & Zwicky 1947) are stars that were originally part of a binary that was disrupted either when the other star in the binary exploded as a supernova (the Hills mechanism, Hills 1983) or due to dynamical three- or four-body interactions (Hut & Bahcall 1983; Hoffer 1983). The disruption of the binary system results in runaway stars having peculiar velocities greater than $30 \, \mathrm{km \, s^{-1}}$ (Renzo et al. 2019). Since most of the O/B stars are located close to the Galactic plane (Maíz-Apellániz 2001) and given the young characteristic age of the pulsar, it would have to be born close to its current position. Thus, the progenitor of the pulsar would have to be a runaway star to be able to reach its current observed position. If we can confirm that the position of the pulsar as predicted by the NE2001 model is accurate, this would be the first known pulsar whose progenitor was a runaway star.

This paper is structured as follows. In Section 2, we describe the discovery and timing of PSR J0837–2454, and our observations and analysis of the data collected with ATCA. In Section 3, we present the results from the timing and interferometric analysis. In Section 4, we discuss the implications of our results and present the conclusion in Section 5.

## 2. Observations and Data

### 2.1. Discovery and Timing of PSR J0837–2454

PSR J0837–2454 was discovered as part of the High Time Resolution Universe (HTRU) intermediate-latitude survey (HTRU; Keith et al. 2010) carried out with the Parkes Radio Telescope in both the single-pulse and periodicity pipelines (Burke-Spolaor et al. 2011). No period has previously been reported for this pulsar. Its timing solution, derived as described below, is shown in Table 2.

After its discovery, temporally resolved spectra ("search data") were obtained for this pulsar from the time of its discovery in 2011, until early 2017. For this period of time, the pulsar was not observed using standard timing observations ("folded data"), because of the difficulty in obtaining a coherent timing solution. This was due largely to its large red noise properties, and in part to its inaccurate position and large period derivative (which initially quickly made the pulsar lose phase coherence). All search data were collected at frequencies within the 1.1–1.5 GHz band using the Berkeley Parkes

Swinburne Recorder (BPSR; Keith et al. 2010), HI-Pulsar (HIPSR; Price et al. 2016), and Digital Filterbank 4 (DFB4; Ferris & Saunders 2004) instruments; this data is available for download from CSIRO's online Data Access Portal.[12] After flagging of interference-affected channels, the average frequency of most data, and the reference frequency we used for timing, was 1382 MHz.

We measured an initial timing solution using single-pulse events from all epochs. It was then noted that the pulsar was also visible in a Fourier search; to obtain TOAs with higher stability (i.e., not subject to the pulse-to-pulse variations that are well-known to occur in pulsars), each observation was then averaged over the rotational period of the pulsar ("folded") using that single-pulse solution. A time-of-arrival (TOA) was measured separately for each observation, using the DSPSR (van Straten & Bailes 2011) and PSRCHIVE (Hotan et al. 2004) software. TOA creation requires comparing new observations to a standard template. We first tried timing all data against a rudimentary template created from a subset of the data, summing all detections over the time period from 2011 June to September. A template used in this way is not ideal, as the cross-correlation of noisy data with a template made with that same data results in erroneously low TOA errors. Thus, we used an analytic template, which we obtained as described below.

We first aimed to produce a higher-S/N integrated profile with which to fit a representative analytic template. As with many young pulsars, PSR J0837–2454 is dominated by large amounts of red noise (e.g., Shannon & Cordes 2010). Thus, we were only able to obtain a low rms timing solution (rms residuals 613 $\mu$s) over a subset of data in the time frame of 2012 January to 2015 September, fitting for R.A., decl., $F$, $\dot{F}$, and $\ddot{F}$ (which correspond to R.A., decl., pulsar spin frequency, frequency derivative, and second frequency derivative, respectively). We integrated the folded data across the BPSR/HIPSR data during these epochs to obtain a high-S/N profile. These data, integrated over that entire time span, produce the profile seen in Figure 1. To that profile, we fit an analytic template and rederive TOAs and a timing solution for all data. The analytic template consisted of four Gaussian components, and its subtraction from the data left the noise-like residual shown in gray in Figure 1.

Due to the significant red noise observed in this pulsar (large power in low-order terms; see Figure 2), we employed the method of Coles et al. (2011) to solve for the pulsar parameters using a generalized least-squares approach. We used the SPECTRALMODEL plugin of the TEMPO2 timing software to model the red noise as a power law with spectral index of −6, typical of the steep red noise process commonly seen in young pulsars.

In the residuals that result from the final timing solution, there is clearly a large cubic term apparent in the data that causes the pulsar's rotation to vary greatly during our several-year data span. The rms residual variance in our final timing solution is 90 ms, which is dominated by the red noise (individual TOA error bars are on the order of 10 $\mu$s, and as previously noted a timing solution over a subset of the full time span resulted in an rms residual variance of a more reasonable 613 $\mu$s).
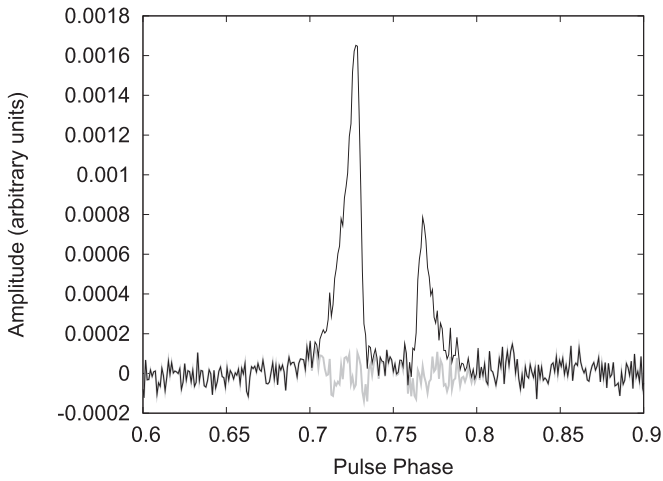
---

**Figure 1.** In black we show the integrated profile of PSR J0837–2454 at a reference frequency of 1382 MHz for the BPSR/HIPSR data over the period 2012 January–2015 September. The gray line shows the result of subtracting our analytic timing template from this integrated profile. For clarity of this figure, the analytic template is not shown.
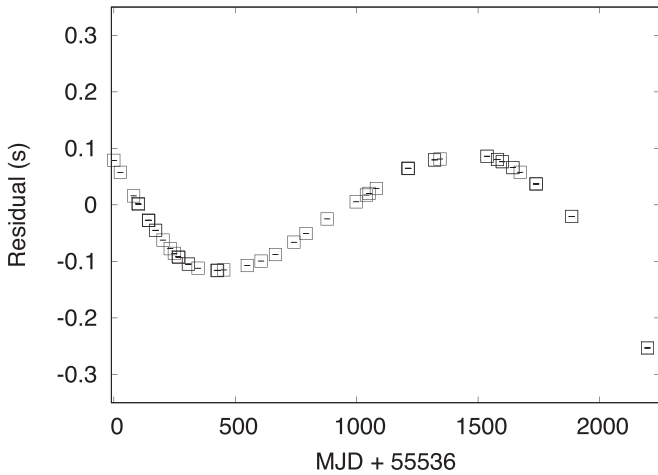


**Figure 2.** Here we show the residuals following the timing procedure described in Section 2.1. A clear cubic term, encompassing part of the red noise exhibited by this pulsar, is clear. The error bars are plotted but are sufficiently small ($<10\ \mu$s) such that they are not clearly visible on this plot.

The observed and derived parameters from our observations and from our timing solution are presented in Table 1.

### 2.2. ATCA Observations and Data Reduction

We used the Australia Telescope Compact Array (ATCA) in the 1–3 GHz band to observe the field of PSR J0837–2454 and search for any supernova remnant (SNR) that might be associated with the pulsar. We were awarded 24 hr, split into two observing sessions of 12 hr each. The first of these sessions was conducted on 2011 November 4 with the array in 750C configuration. The second was on 2012 March 4 with the array in EW352 configuration. These observations provided a balance between a large field of view and ideal frequency placement to detect what would be a nonthermal power-law spectrum of the SNR. The observations were centered on an early solution for the position of the pulsar, R.A. 08:37:57.76 and decl. −24:54:30.51 (J2000 epoch), which has a small offset of 0.08 s in R.A. from the final timing solution reported in Table 2.

**Table 1**
Timing Solution for PSR J0837–2454

| Parameter | Value (err) |
|---|---|
| **Measured Parameters** | |
| R.A. (J2000) | 08:37:57.73(6) |
| Decl. (J2000) | −24:54:30(1) |
| Galactic longitude (°) | 247.58 |
| Galactic latitude (°) | 9.77 |
| DM (pc cm$^{-3}$) | 143.1(1) |
| $P$ (ms) | 629.41024(2) |
| $\dot{P}$ ($\times 10^{-13}$ s/s) | 3.490(2) |
| $F$ (1/s) | 1.58878890(5) |
| $\dot{F}$ (1/s$^2$) | $-8.808(4) \times 10^{-13}$ |
| **Derived Parameters** | |
| $\tau_c$ (kyr) | 28.6 |
| $B_{surf}$ (G) | $1.5 \times 10^{13}$ |
| $\dot{E}$ (erg s$^{-1}$) | $5.5 \times 10^{34}$ |
| DM distance (NE2001) | 6.29 kpc |
| $z$-height (NE2001) | 1.1 kpc |
| DM distance (YMW17) | >25 kpc |
| $z$-height (YMW17) | … |
| **Reference Values** | |
| Reference frequency (MHz) | 1381.999 |
| Reference epoch (PEPOCH, MJD) | 55588.628331 |
| TOA range (MJD) | 55536-57787 |
| Solar system ephemeris | DE405 |
| Units | TCB (tempo2) |

We used J1934–638 as an ATCA standard primary calibrator and J0843–259 as the phase calibrator for both the observing sessions. A total of ∼1.5 hr across the two sessions were spent observing the primary calibrator. We spent a net sum of ∼4 hours observing the phase calibrator; those observations were interleaved with on-source observations. This leaves a total of 18.5 hr on-target. Both the sessions were carried out with a center frequency of 2.1 GHz, and 2048 frequency channels, with each channel 1 MHz in width. This setup allows us to detect structures in the combined data from a smallest angular resolution of ∼5″8 to spatial scales as large as ∼15′8, with a field of view of ∼22′3.

The data calibration and image processing was done using the CASA software package. The data from each epoch were manually flagged before being manually calibrated using standard CASA procedures.[13] The calibrated data from both observing sessions were concatenated into a single data set. This concatenated data set was then deconvolved and cleaned using CASA's CLEAN routine.

We deconvolved the data using two different weighting techniques corresponding to the type of information we required from the image. First, we deconvolved the image using the uniform weighting scheme implemented in CASA. This type of weighting returns an image of the sky with the best resolution, but with a reduced sensitivity. The image produced with uniform weighting is shown in Figure 3. This image has an rms flux of $\sigma = 24\ \mu$Jy.

We also produced an image using the Briggs weighting (Briggs 1995) scheme in CASA, with the robustness parameter $R = 0$. This weighting gives a good trade-off between resolution and sensitivity, which allows us to search for a supernova remnant
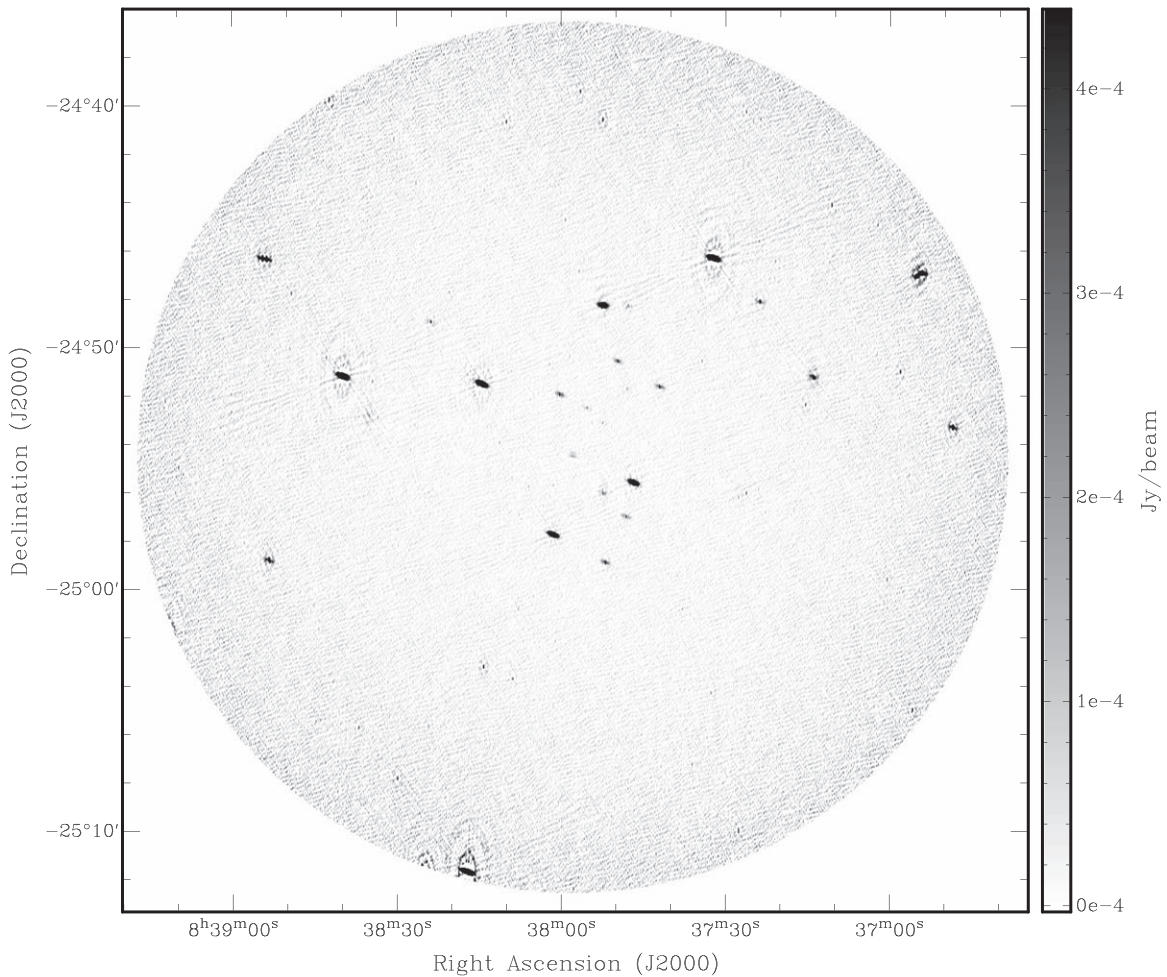
---

**Figure 3.** Image produced using uniform weighting in the deconvolution process. This image provides the highest spatial resolution but has a reduced average signal-to-noise ratio. This type of weighting is ideally suited for identifying point sources in the field of view. The pulsar PSR J0837−2454 is weakly visible at the center of the image.

over a suitably large range of angular resolutions. This image is shown in Figure 4. This image has an rms flux of $\sigma = 32\,\mu$Jy. Our sensitivities improve on the archival NVSS imaging of this field (Condon et al. 1998) by a factor of more than 14.

## 3. Results

### 3.1. Properties of the Pulsar

This pulsar stands out in several ways. First, its emission is highly modulated, with single pulses visible at a level of several hundreds of mJy, while the mean profile flux density is ~80 $\mu$Jy. We do not have sufficient S/N in our observations to assess whether there are any extended periods of nulling in the pulsar.

Using our highest-S/N observation, we measured the DM to be $143.1 \pm 0.1\,\mathrm{pc\,cm^{-3}}$. We also measured DM as a function of time (separately for each independent observation) and found no significant deviations within our measurement errors.

The pulsar is relatively young, and is at around the 13th percentile for young pulsar ages compared to cataloged pulsars with measured characteristic ages. The most striking thing about this pulsar is its large apparent height above the Galactic plane based on the NE2001-implied distance compared to the age of the pulsar. Given our measured DM, we can estimate the distance to the pulsar, $D$, based on the known Galactic free electron density, $n_e$, along the line of sight. Currently, the two most broadly used

models of the Galactic free electron density, $n_e$, are the NE2001 model (Cordes & Lazio 2002) and YMW (Yao et al. 2017) model. The distance prediction by the NE2001 model results in a radial distance $D_{\mathrm{cl}} = 6.3$ kpc, implying a height of this pulsar above the Galactic plane of 1.1 kpc. The prediction from the YMW model indicates that there are only 118 pc cm$^{-3}$ of Galactic DM in this direction, and thus puts the pulsar at the edge of the Galaxy (or, extragalactic, which is not likely, providing a prediction that the pulsar comes from a distance of $D_{\mathrm{ymw}} = 151$ Mpc). In Figure 5, we show the radial and orthogonal offset from the Galactic center for this pulsar, young pulsars ($\tau_c < 50$kyr) and all pulsars as inferred from the DM-derived distances based on the NE2001 electron density model. While it is clear that this pulsar inhabits a somewhat sparsely populated position in the Galactic plane (specifically it is located well above the outer/Perseus arm of the Galaxy), the position in reference to the Galactic center is even more pronounced when considering the young pulsar population that is comparable in characteristic age to this pulsar.

Most pulsars are born in supernova explosions in the disk of the Galaxy, and the explosive birth of a pulsar can impart a kick to the pulsar at birth, resulting in a high transverse velocity. Due to this kick, pulsars gradually migrate out of the plane of the Galaxy and populate the high latitude regions (i.e., the halo) of the Galaxy. The presence of a young pulsar, PSR
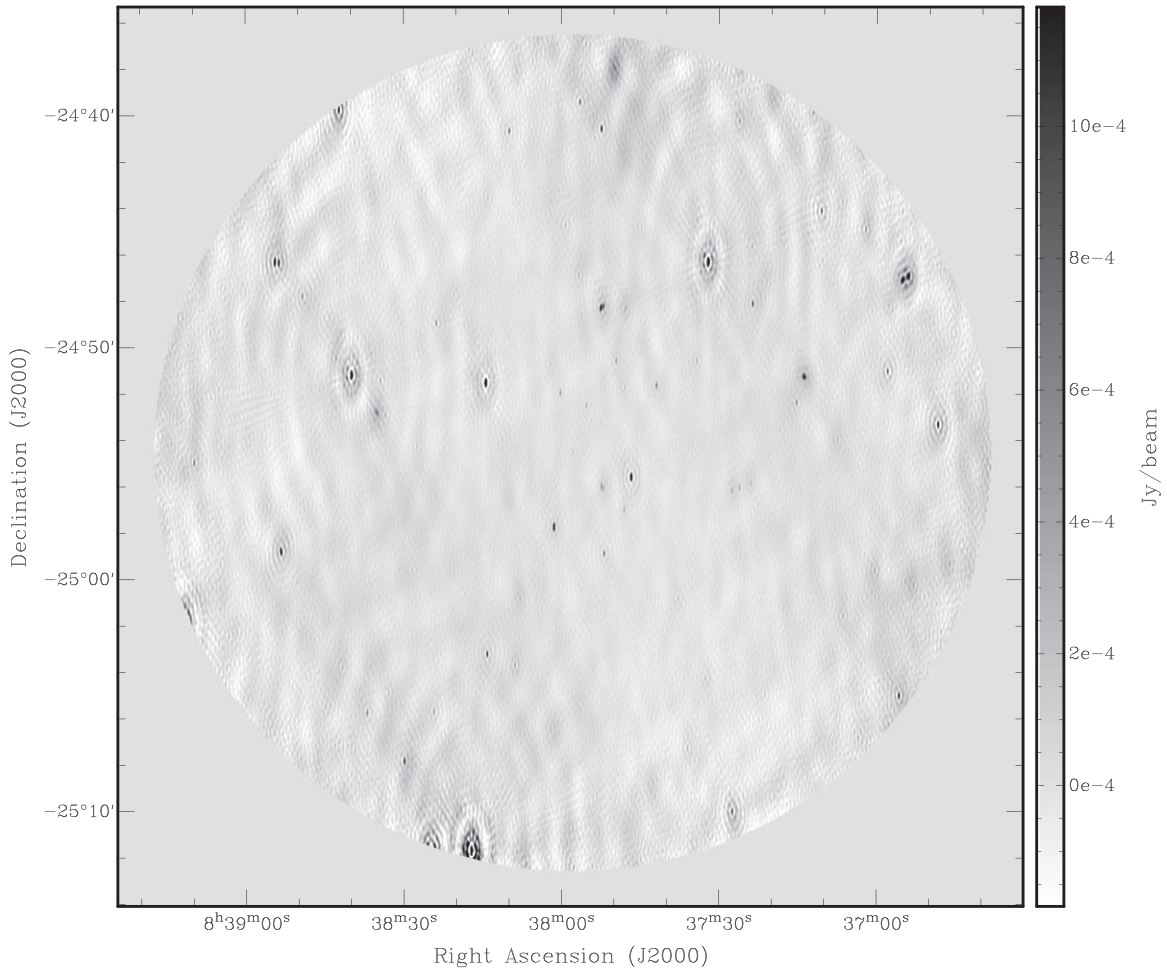
**Figure 4.** Image produced using Briggs weighting with robust parameter $R = 0$ in the deconvolution process. This image provides a good trade-off between spatial resolution and sensitivity, allowing us to search for a supernova remnant over a large range of spatial resolution. We do not detect any supernova remnant associated with PSR J0837–2454 in this image.

J0837–2454, in the outer regions of the plane, as visible in Figure 5 is therefore surprising.

### 3.2. Objects in the ATCA Field of View

We detect a point source at the position of PSR J0837–2454 in both observing sessions. We also detect it in the concatenated data, with a flux of $0.18 \pm 0.05$ mJy ($5.4\sigma$ significance). This flux density is consistent with that of the mean (continuum, nonpulsed) pulsar emission measured by Parkes telescope, if we use a duty cycle of $\sim 5\%$ that encompasses only the two emitting peaks of the pulsar's profile.

We do not detect any extended emission in our ATCA data down to a level of 3 times the rms image noise (equivalent to 96 $\mu$Jy beam$^{-1}$) that might represent the existence of a compact SNR or pulsar wind nebula (PWN) around the pulsar. This nondetection places a conservative upper limit on the flux density of any non-pointlike features associated with the potential low-surface-brightness SNR of the GLEAM image (see Section 3.3.1).

We identified all the point sources in the uniform weighted image, associating them with any known sources in NED[14] and SIMBAD (Wenger et al. 2000). To identify objects in our field,

we searched for point sources in the image with flux densities above $5\sigma$, where $\sigma = 24.43$ $\mu$Jy is the rms flux in the image. All of these sources, both with and without known associations in the NED and SIMBAD catalogs, are listed in the supplemental information provided with this paper.

### 3.3. A Search of Archival Data

#### 3.3.1. GLEAM Survey

We obtained images from the Galactic and Extragalactic All-sky MWA Survey (GLEAM; Hurley-Walker et al. 2017) for this sky position.[15] Figure 6 shows a wide-field view of the stacked 170–231 MHz images in this region, which exhibits a highly diffuse, semisymmetric structure surrounding the pulsar position.

Since the structures in the image have not been deconvolved due to a lack of multiscale CLEAN when the images were generated, the choice of a background is essential in performing a peak brightness measurement across frequency to measure a spectral index for this structure. However, this is severely hampered due to the poorly defined edges of the source, as well as strong contamination from the large number of extragalactic sources in the image. As a result, it is hard to
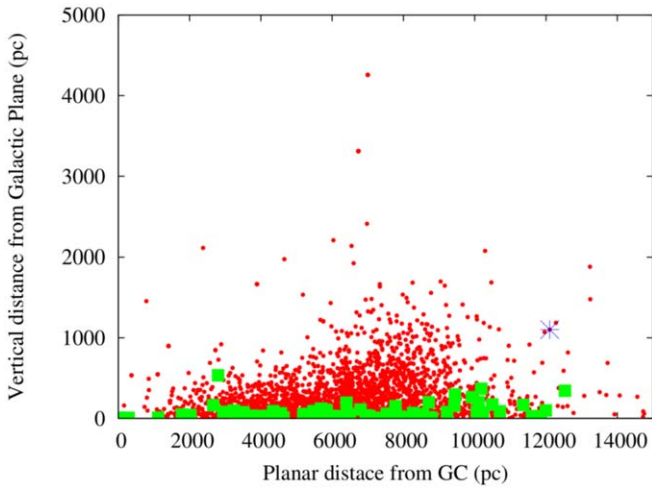
---

**Figure 5.** Here we show the positions of pulsars in the Galaxy relative to the Galactic Center (GC). The vertical axis represents the absolute value of the pulsar's $z$-height, while the horizontal axis represents the planar distance from the GC. For this plot we have assumed a GC-Sun distance of 8122 pc, and drawn the galactic longitude and latitude ($gl$ and $gb$, respectively) and NE2001-derived dispersion measure distance from PSRCAT. All pulsars are shown as small red circles, pulsars of characteristic age less than 50 kyr are shown as larger green squares, and PSR J0837–2454 is shown as a blue asterisk.
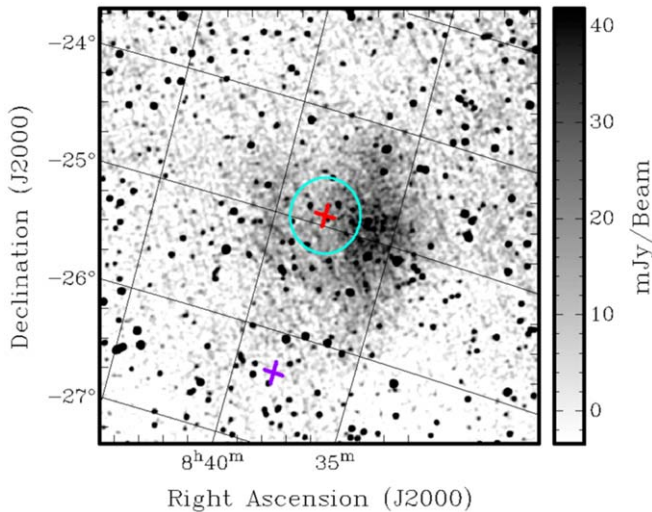


**Figure 6.** A wide-field view of the pulsar's position in the stacked 170–231 MHz GLEAM data. The cyan circle shows the size of the image in Figures 3 and 4. The crosses are of arbitrary size, and show the positions of pulsars PSR J0837–2454 (red) and PSR J0838–2621 (purple).

estimate the spectral index of the source with any amount of confidence. Consequently, the GLEAM data does not provide conclusive evidence of the diffuse structure being an SNR associated with PSR J0837–2454.

### 3.4. Southern Hα Sky Survey (SHASSA)

We obtained images from the Southern Hα Sky Survey (SHASSA; Gaustad et al. 2001) for this sky position to search for associated Hα emission from this region. The SHASSA image for this portion of the sky is shown in Figure 7, with the position of PSR J0837–2454 shown by the red cross and the cyan circle shows the size of the images in Figures 3 and 4. As we can see, the location of PSR J0837–2454 is coincident on the sky with a

diffuse Hα filament, with a photon flux amplitude of $\mathcal{R} = 470$ Rayleigh in the pixel at the position of the pulsar. The morphology of the surrounding Hα emission is inconsistent with the GLEAM diffusion emission morphology and thus we cannot conclusively claim that the two are related to each other.

### 3.5. Other Archival Data

To search for other counterparts to the diffuse emission detected with the GLEAM survey, we obtained an image for this part of the sky from the TIFR GMRT sky survey[16] (TGSS; Intema et al. 2017), which is at a center frequency of 150 MHz. This image did not show evidence for any supernova remnant (Figure 8).

It is not surprising that the features were not visible in the TGSS (and ATCA) observations. The 150 MHz TGSS image, shown in Figure 8, has a comparable observing frequency to GLEAM (Intema et al. 2017) and similar rms noise levels of a few mJy. However, in the case of both ATCA and TGSS, it is likely that they did not have sufficient u,v coverage to detect the diffuse structures found in GLEAM, which has ample sensitivity on short baseline spacings. Thus, with ATCA, TGSS, and GLEAM, we are probing the region around PSR J0837–2454 at drastically different spatial scales and frequency bands; it is clear based on TGSS and ATCA that the structure appears to be truly diffuse on scales approximately greater than a few arcminutes, thus lacks sharp filamentary structure.

We did not find any emission associated with the GLEAM source in other wavelength bands using the ALADIN (Bonnarel et al. 2000) sky atlas. The Chandra and XMM-Newton X-ray satellites do not have coverage for this portion of the sky. An analysis with the latest data from the Fermi Large Area Telescope (Atwood et al. 2009), accessed from the Fermi Science Support Center[17] (Acero et al. 2015), also did not show evidence for a supernova remnant.

### 4. Discussion

#### 4.1. Expectations

Young pulsars like PSR J0837–2454 are often associated with an SNR or a PWN. In Figure 9, we plot the Galactic $z$-height for all pulsars with a characteristic age $\tau_c \leqslant 100$ kyr, highlighting the pulsars associated with an SNR/PWN. We can see that PSR J0837–2454 has an anomalously high $z$-height as compared to other pulsars of similar age. Of the 74 pulsars with characteristic age $\tau_c \leqslant 28.6$ kyr, 59 (i.e., 79.7%) are associated with either an SNR or PWN.

It is notoriously difficult to predict the properties of any potential SNR with any certainty. The PWN will typically be constrained to the region close to the pulsar, while the SNR will be more extended with a diameter ranging anywhere from a few tens of arcseconds to a few degrees, depending on the expansion velocity, its stage of evolution, and the magnetic field and density of the interstellar medium. Even though the size and morphology of the SNR might be difficult to predict, assuming the characteristic age of PSR J0837–2454 is a reasonable approximation of the age of the pulsar, we can expect the pulsar to be in the late Sedov expansion phase (Sedov 1959) or early radiative phase (Cioffi et al. 1988).

---

[16] https://vo.astron.nl/tgssadr/q_fits/cutout/form
[17] The data access page can be found at the link: https://fermi.gsfc.nasa.gov/ssc/data/.
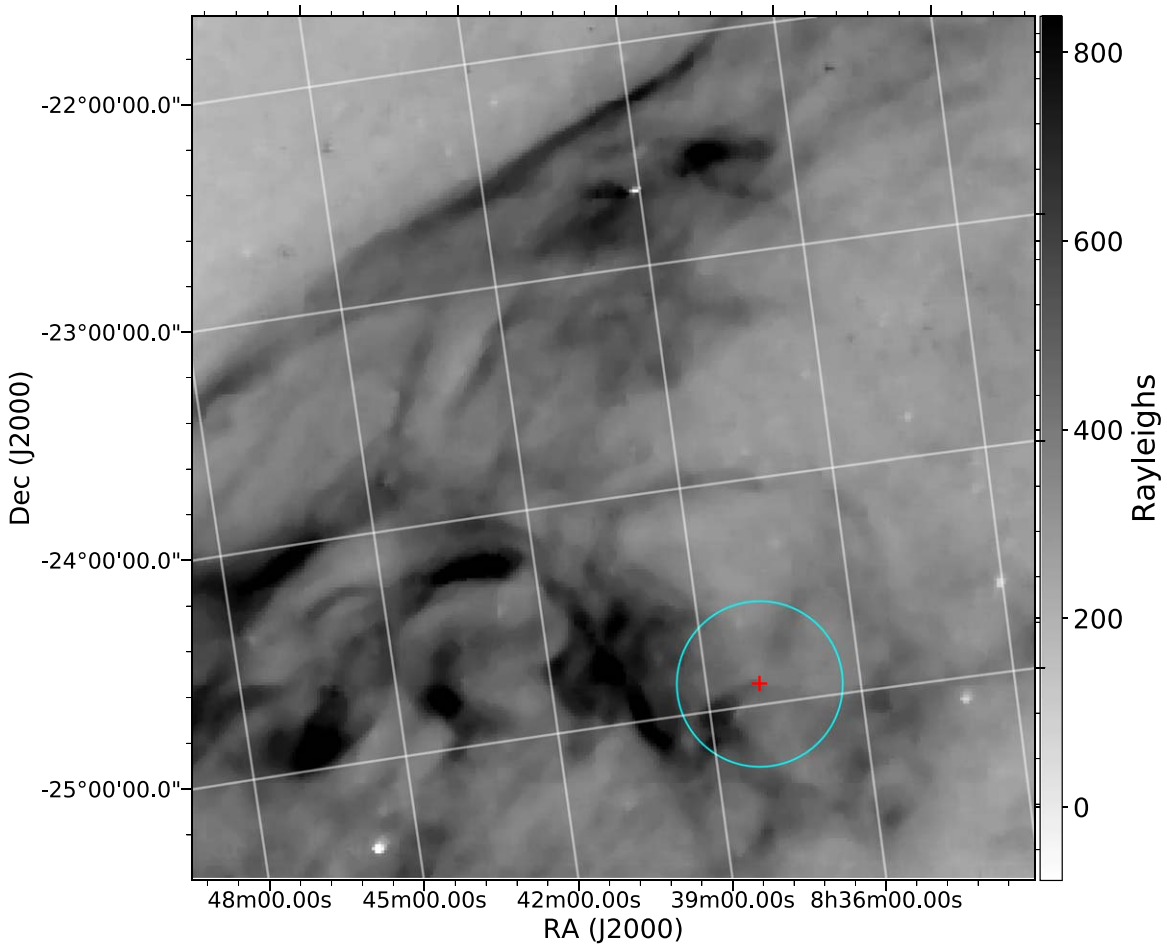
**Figure 7.** A wide-field view of the position of PSR J0837–2454 obtained from the Southern Hα Sky Survey (SHASSA). The position of the pulsar is shown by the red cross, while the cyan circle shows the size of the image in Figures 3 and 4.

### 4.2. Is the GLEAM Source an Associated Supernova Remnant?

As discussed in Section 3, we do not detect an SNR in our ATCA observations; however, on a larger scale we detect extended emission in the lower-frequency GLEAM data. This emission is concentrated around PSR J0837–2454 and shows morphology consistent with a diffuse, low-surface-brightness SNR.

As described in Section 3.3.1, we could not effectively assess the spectral index of this diffuse feature with the GLEAM data, thereby preventing us from making a conclusive statement about whether the diffuse source is the SNR. While PSR J0837–2454 is also surrounded by Hα emission (see Section 3.4), the difference in the morphology of the Hα emission and the GLEAM diffuse emission suggests different origins for these two features. Thus, given the available data, we cannot confirm if the GLEAM diffuse emission is an SNR.

### 4.3. Limit on the Distance to the PSR/SNR Association

Despite the lack of a confirmed SNR around PSR J0837–2454, we can set limits on the distance to the pulsar using the observational evidence obtained from the SHASSA and GLEAM data and compare it to the one derived using the NE2001 model (Cordes & Lazio 2002). A distance discrepancy, if it exists, is not an unusual occurrence in pulsar distance estimation (see, for example, Chatterjee et al. 2009; Deller et al. 2009). In particular, Chatterjee et al. (2009) showed that the NE2001 model can overestimate the distances to some pulsars, with a striking example
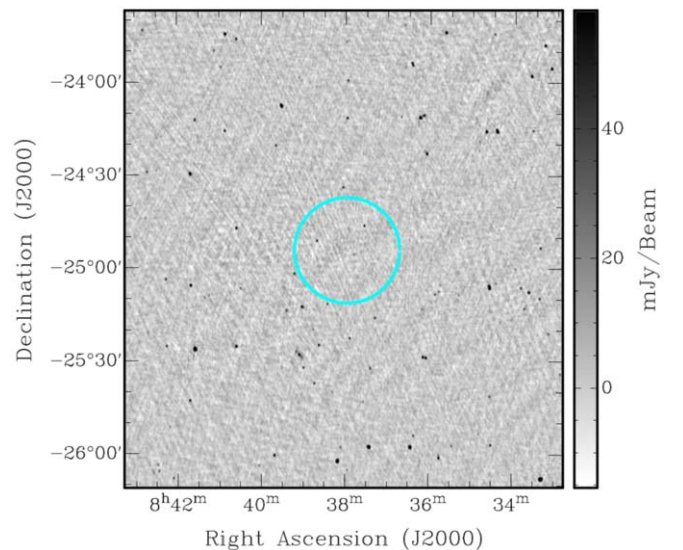


**Figure 8.** The 150 MHz TGSS image in the region of PSR J0837–2454. The cyan circle shows the size of the image in Figures 3 and 4.

of the DM-derived distance to PSR B0450–18 being a factor of ∼3 greater than the parallax distance. It is possible that the YMW model also suffers from similar overestimation of distances to pulsars as the NE2001 model. If the NE2001 model overestimates the distance to PSR J0837–2454, that might explain why PSR
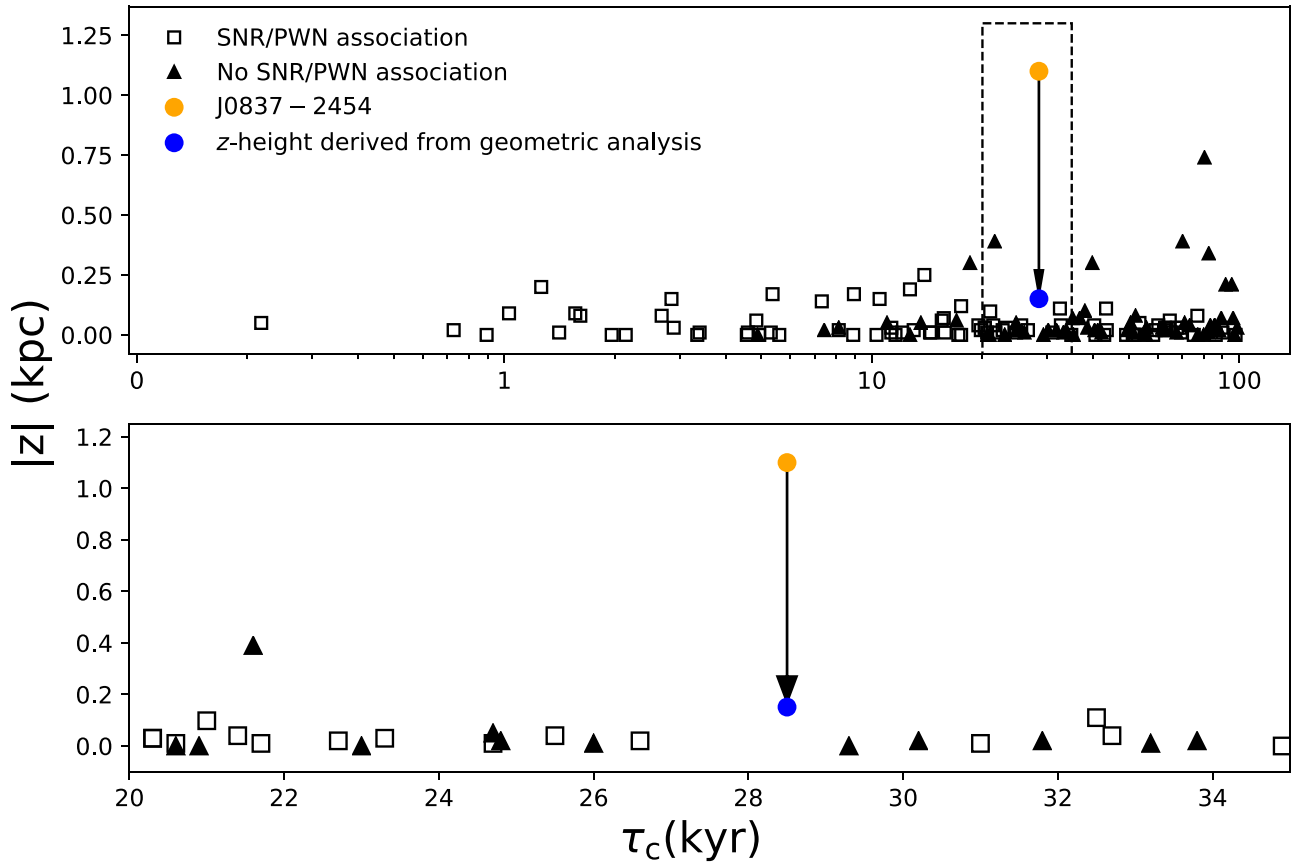
**Figure 9.** The absolute z-height of pulsars, inferred from the NE2001 model and their DMs, with $\tau_c \leqslant 100$ kyr, is plotted against their characteristic age in the top panel. The position of PSR J0837–2454 based on the NE2001-derived z-height is shown with an orange dot. The position of PSR J0837–2454 based on the geometric analysis in Section 4.3 is shown with a blue dot. The bottom panel shows a zoom-in around the position of PSR J0837–2454, shown with the rectangle in the top panel. We can see that the NE2001-derived z-height of PSR J0837–2454 is anomalously high compared to other pulsars of similar characteristic age. We can also see that many of the pulsars with similar age as PSR J0837–2454 have an SNR/PWN associated with them.

J0837–2454 is so unusual in its Galactic position relative to other young pulsars (see Figures 5 and 9).

### 4.3.1. Using SHASSA Hα Emission

As described in Section 3.4, PSR J0837–2454 is colocated with a diffuse Hα emission complex. Some of this Hα complex also lies along the line of sight to the pulsar and could be contributing to the observed DM for the pulsar. This excess DM could lead to an overestimated distance, thereby over-estimating the z-height of the pulsar. Since the NE2001 model does not list any overdensities or clumps in the free electron density in the direction of this pulsar (Cordes & Lazio 2002), it is not implicitly accounting for any excess DM that might be originating from the observed Hα complex.

From Figure 7, the amplitude of the Hα emission from the pixel coincident with PSR J0837–2454's position is $\mathcal{R} = 470$ Rayleigh. Following the discussion in Kulkarni et al. (2014; their Section 4.4), the SHASSA photon flux in Rayleighs can be converted to an emission measure, EM = $\mathcal{R} \times 2.2$ pc cm$^{-6}$ = 1034 pc cm$^{-6}$. However, since we do not know the length of this Hα complex along the line of sight, it is not possible to directly convert this EM to its corresponding free electron density or a dispersion measure contribution.

Instead, we can place limits on the distance to PSR J0837–2454 using a method similar to the one used in Bannister & Madsen (2014). Given a free electron density, $n_e$, a filling factor, $f$, and the distance to the pulsar, $D_p$, the dispersion measure can be calculated as, DM = $n_e f D_p$. Similarly, the EM can be calculate as, EM = $n_e^2 f\, D_{H\alpha}$, where $D_{H\alpha}$ is the length of the Hα complex.

We can infer the approximate Galactic free electron density along the line of sight to the pulsar by dividing the DM estimated by the NE2001 model by the corresponding distance associated with this DM. This leads to a free electron density approximately an order of magnitude lower than the average midplane density of $\approx 0.1$ cm$^{-3}$. Correspondingly, the Galactic estimate of the EM in this direction is negligible compared to that measered by SHASSA. Thus, we can assume that most of the observed DM and EM is a result of the Hα complex along the line of sight. Assuming an approximately constant free electron density and filling factor in the this Hα complex, the distance to the pulsar can be written as (Bannister & Madsen 2014),

$$D_p = \frac{DM}{\sqrt{EM}} \frac{\sqrt{D_{H\alpha}}}{\sqrt{f}}. \qquad (3)$$

Rearranging the above equation and using the measured values of DM = 143 pc cm$^{-3}$, EM = 1034 pc cm$^{-6}$, and normalizing to a filling factor value of $f = 0.1$, we find that

$$\frac{D_p}{D_{H\alpha}} = 14 \left( \frac{0.1}{f} \right)^{1/2} (D_{H\alpha})^{-1/2}. \qquad (4)$$

Assuming the Hα complex fills the entire path along the line of sight to the pulsar, i.e.,

$$\frac{D_{\mathrm{p}}}{D_{\mathrm{H}\alpha}} \sim 1, \tag{5}$$

gives us an estimate of the distance to the pulsar,

$$D_{\mathrm{p}} \approx 0.2 \left(\frac{0.1}{f}\right)^{1/2} \mathrm{kpc}. \tag{6}$$

This distance is significantly smaller than that predicted by the NE2001 model ($D_{\mathrm{cl}} = 6.3$ kpc). This distance corresponds to a z-height of $\approx 34$ pc, which is consistent with those observed for other young pulsars like PSR J0837−2454.

However, if the Hα complex does not fill the entire distance out to the pulsar, as we assumed in this analysis, then given the small Galactic free electron density along this line of sight, the pulsar could be much further away than the distance calculated above. This effect would also dominate the changes in the distance estimate arising from differences in the assumed filling factor for the Hα complex.

### 4.3.2. Using GLEAM Diffuse Emission

If we assume that the diffuse emission observed in the GLEAM data is indeed the SNR, then we can infer a limit on the distance to PSR J0837−2454 by using the average velocity of expansion of the SNR shell in different stages of evolution. From Figure 6, an angular radius that visually encloses most of the SNR emission can be approximated as $\theta \sim 0°7$. Using the small angle approximation, the spatial radius of the SNR will be $R = D \times \theta$, where $D$ is the distance to the pulsar–SNR system. We also know that the approximate age of the pulsar–SNR system is $\tau_{\mathrm{c}} = 28.6$ kyr. Next, we assume an initial ejecta velocity of $v_{\mathrm{e}} = 5000$ km s$^{-1}$ for our SNR in the ejecta-driven phase lasting $t_{\mathrm{e}} \simeq 1$ kyr and a typical $v_{\mathrm{s}} = 200$ km s$^{-1}$ during the 27.6 kyr since then, which the SNR has spent in the Sedov expansion phase (Alsabti & Murdin 2017). Combining the two velocities, we get a velocity estimate that is weighted by the duration of time spent in each evolutionary phase of

$$\bar{v} = \frac{v_{\mathrm{e}}(t_{\mathrm{e}})}{\tau_{\mathrm{c}}} + \frac{v_{\mathrm{s}}(\tau_{\mathrm{c}} - t_{\mathrm{e}})}{\tau_{\mathrm{c}}} \approx 370 \text{ km s}^{-1}. \tag{7}$$

Using the average velocity and time for which the SNR has been expanding, we can determine the distance to the SNR:

$$D = \frac{\bar{v}\tau_{\mathrm{c}}}{\theta}. \tag{8}$$

Assuming the values previously noted, we determine a distance of

$$D \approx 0.9 \left(\frac{\bar{v}}{370 \text{ km s}^{-1}}\right)\left(\frac{\tau_{\mathrm{c}}}{28.6 \text{ kyr}}\right)\left(\frac{0°7}{\theta}\right) \text{kpc}. \tag{9}$$

This distance also differs significantly from the predictions made using the NE2001 model ($D_{\mathrm{cl}} = 6.3$ kpc).

The above analysis is based on simple constant weighted velocity and geometric arguments and is independent of the Galactic free electron density in that direction in the Milky Way. As such, it provides an independent estimate of the distance to the pulsar–SNR system. As we discuss below, for the distance derived from this analysis to agree with the distance derived from the NE2001 model, the SNR ejecta

would need to have a much higher average velocity, or the pulsar and SNR would have to be much older than the derived characteristic age. Another way in which this distance discrepancy could be resolved is if the diffuse GLEAM source is not in fact the SNR.

Fixing the distance in Equation (8) to be equal to that predicted by the NE2001 model, i.e., $D = D_{\mathrm{cl}} = 6.3$ kpc and assuming the characteristic age is a reasonable approximation, that implies that the average velocity of the SN ejecta over the past 28.5 kyr would have to be approximately 2600 km s$^{-1}$. This average velocity implies, using Equation (7) and the same assumption of $v_{\mathrm{e}} = 5000$ km s$^{-1}$ for our SNR in the ejecta-driven phase lasting $t_{\mathrm{e}} \simeq 1$ kyr, that the ejecta would need to be moving at a velocity of $\sim 2500$ km s$^{-1}$ in the post-ejecta-driven phase. This velocity seems uncharacteristically high for ejecta that are out of their ejecta-driven phase (Alsabti & Murdin 2017) and thus is unlikely to be representative of the true velocity of the ejecta. Based on these arguments, a distance much smaller than that predicted by the NE2001 model is preferred for the pulsar–SNR system.

Similarly, to be consistent with the distance estimate from the NE2001 model, the pulsar–SNR system would have to be a factor of $\sim 7$ older than the characteristic age. It is not unusual for a pulsar to have a true age to be significantly different from the characteristic age. For example, PSRs B1951+32 and B0538+2817 have true ages that are a factor of 0.5 and 0.05 smaller than their characteristic ages, respectively (Migliazzo et al. 2002; Kramer et al. 2003, respectively). Another example of such a discrepancy is PSR J1801−2451, where the pulsar's proper motion suggests that the true age of this pulsar could be significantly higher than its characteristic age (Zeiger et al. 2008). Two sources of uncertainty in the calculation in the characteristic age (Equation (1)) are the braking index, $n$, and the period derivative, $\dot{P}$. In our calculation, we assumed $n = 3$, though it is possible that the braking index for this pulsar might be significantly different (Noutsos et al. 2013). To get an age that is a factor of $\sim 7$ greater than that we calculate in Equation (2), the braking index would have to be $n \approx 1.3$, which seems unlikely, given that only the Vela pulsar ($n \approx 1.4$, Lyne et al. 1996) and PSR J1734−3333 ($n \approx 1$, Espinoza et al. 2011) have been measured to have such low braking indices. Finally, we might be underestimating the characteristic age if we were overestimating the period derivative, $\dot{P}$, of the pulsar. This is possible given that the period derivative can be contaminated by the kinematic motion of the pulsar, in what is known as the "Shklovskii effect" (Shklovskii 1970). The contribution from the kinematic terms is usually small for pulsars like PSR J0837−2454, but given its unique location in the Galaxy, these effects might be significant enough to resolve the distance discrepancy with the NE2001 model described above. If the pulsar indeed turns out to be significantly older, there are 12 pulsars with characteristic ages greater than 100 kyr that have a supernova remnant associated with them, so it might still be possible to detect emission from this SNR.

Assuming that a distance of $D = 0.9$ kpc is an accurate estimate of the true distance to PSR J0837−2454, we can calculate the z-height of the pulsar above the Galactic plane to be $z_{\mathrm{new}} = D \times \sin(b)$, where $b$ is the latitude of PSR J0837−2454. Doing the calculation, we get a new z-height for PSR J0837−2454 of $z_{\mathrm{new}} \approx 151$ pc. This new z-height is much more reasonable than the z-height predicted by the NE2001 model shown in Figure 9. This new z-height places it among other known pulsars of similar ages, as shown in Figure 9.

### 4.4. What If the NE2001 Position Is Accurate?

It is likewise possible that the diffuse GLEAM object is not a supernova remnant, and/or not associated with the pulsar's origin. As noted in the previous section, if the pulsar is indeed as distant as the DM models imply, any associated SNR would be expected to be at a location and size detectable by ATCA. In this scenario, we obviously did not detect the SNR, so we discuss here a few reasons why one might not have been detected, as well as the implications of a pulsar detected this far from the Galactic plane.

#### 4.4.1. Implication of Position of PSR J0837–2454

If accurate, the NE2001-derived position of PSR J0837–2454 makes it unique among the known population of young pulsars in the Milky Way (see Figure 9). Given the large period and period derivative of the pulsar, it is not a recycled pulsar and was likely born from a core-collapse supernova from an O/B-type star. These massive stars are located in the disk of the Galaxy with a scale height of 34 pc (Maíz-Apellániz 2001). We can estimate the $z$-velocity, $V_z$ (McLaughlin et al. 2002), of the pulsar given its kinematic age, $\tau_k$, and the z-height at which it was born, $z_0$,

$$V_z = \frac{z - z_0}{\tau_k}, \quad (10)$$

where $z$ is the current $z$-height of the pulsar. Assuming the pulsar was born in the plane of the Galaxy, i.e., $z_0 = 0$, the true $z$-height of the pulsar is given by the NE2001-derived distance, $z = z_{cl} = 1.1$ kpc (Table 2), and that the kinematic age is equal to the characteristic age, $\tau_k = \tau_c = 28.6$ kyr, the $z$-velocity of the pulsar is,

$$V_z \approx 3.8 \times 10^4 \left(\frac{28.6 \text{ kyr}}{\tau_k}\right)\left(1 - \frac{z_0}{1.1 \text{ kpc}}\right) \text{ km s}^{-1}. \quad (11)$$

This velocity is more than an order of magnitude greater than the tail of the pulsar velocity distribution (Arzoumanian et al. 2002; Igoshev 2020).

Given the large velocity derived in Equation (11), it is unlikely that the pulsar was born in the plane of the Galaxy and migrated to its current observed position. However, the majority of O/B stars are found to be in binaries (Sana et al. 2012). Most of these binaries are disrupted when one of the members undergoes a supernova explosion (Renzo et al. 2019). Assuming PSR J0837–2454 was born from the surviving massive star in such a disrupted binary, the velocity imparted to the star during the disruption event could have allowed the progenitor O/B star to travel further away from the plane of the Galaxy before itself undergoing a supernova remnant to form PSR J0837–2454. If the progenitor of the pulsar was indeed such a runaway star, then in the most optimistic case, it would have a peculiar velocity of ∼60 km s⁻¹ (Renzo et al. 2019), which when combined with an average lifetime of 30 Myr for O/B stars, would allow the progenitor to travel ≈2 kpc before collapsing to a neutron star. Thus a runaway star hypothesis for the progenitor of PSR J0837–2454 would allow it to have a much more reasonable $z$-velocity by having the pulsar born much closer to its current observed position.

Another way to reduce the $z$-velocity would be if the kinematic (or true) age of the pulsar were significantly larger than the characteristic age of the pulsar, which was already explored in Section 4.3.2. In fact, a combination of a larger kinematic age and the progenitor of the pulsar being the second star in a disrupted binary is also highly possible. This would also relax the condition that the progenitor be a runaway star and allow it to be a "walkaway" star, which are more common than runaway stars and have peculiar velocities ⩽ 30 km s⁻¹ (Renzo et al. 2019). Thus, if the NE2001-derived distance is accurate, this would make this the first pulsar that is known to be born from either a runaway or walkaway progenitor star.

These hypotheses can be verified through a measurement of the velocity of PSR J0837–2454. Because of the large timing residuals, we cannot measure the velocity of the pulsar through timing. Since young pulsars tend to exhibit lots of red noise in their timing, we will need a significant increase in the timing baseline to increase the probability of measuring a velocity through timing. The small flux density of the pulsar also inhibits proper motion and parallax measurements through VLBA, which requires pulsars with a flux density higher than 1.6 mJy (Deller et al. 2019). Similarly, the low flux density would also make it difficult to observe scintillations of the pulsar emission and derive a velocity through interstellar scintillation.

#### 4.4.2. Lack of SNR Emission

Based on the arguments presented above, it is likely that the pulsar was born close to its current NE2001-predicted position. If the characteristic age of the pulsar is a good estimate of the true age of the pulsar, we would have expected an SNR in its late Sedov (Sedov 1959) or early radiative evolution phase (Cioffi et al. 1988). However, in these regions of the Galaxy, it is possible that a low ambient circumstellar density at the position of PSR J0837–2454 could contribute to the formation of a diffuse, low-surface-brightness SNR. Radio emission from SNRs arises from synchrotron emission; the relevant electrons are accelerated by the compression of the ambient magnetic field in the shock front, and the matter expelled from the supernova shocks the circumstellar medium (diffusive shock acceleration; Bell 1978; Blandford & Ostriker 1978). If the density of the circumstellar medium is inherently low, it will inhibit the formation of a shock front; this would serve to both reduce the synchrotron emission from the SNR and to lead to a more diffuse observed structure due to a longer phase of rapid expansion.

As synchrotron radiation from SNRs also requires the presence of an ambient magnetic field, an insufficiently strong field will contribute to a weak synchrotron shock front. During a supernova, the ambient field is amplified to strengths sufficient for synchrotron emission (see Schure et al. 2012; Reynolds et al. 2012, for a review of different amplification processes). Reynolds et al. (2012) analyzed archival supernovae to show that the post-amplified strength of magnetic fields in these SNRs ranged from 25 to 1000 μG, or about 2.5–100 times higher than the diffuse Galactic magnetic field. Sun & Reich (2010) created a map of the galactic magnetic field using the NE2001 thermal electron density model, incorporating the findings of Gaensler et al. (2008). Based on their analysis (see Equation (1) Sun & Reich 2010), the ambient Galactic magnetic field strength around PSR J0837–2454 will be on the order of ∼ 2 μG corresponding to the distance prediction made by the NE2001 model. This magnetic field is approximately five times lower than the ambient magnetic field in the disk of the Galaxy, and would require a highly efficient process to amplify it to the field strengths observed in other supernova remnants. A combination of low circumstellar density and low ambient magnetic field would thus work to lower the expected flux density of any SNR, thus making it much harder to detect.

## 5. Conclusions

We present the timing solution for PSR J0837–2454 using the Parkes radio telescope. The timing solution reveals that this pulsar exhibits red noise, and has a relatively young characteristic age of $\tau_c \approx 28.6$ kyr. Given the young age of the pulsar, we search for a supernova remnant around PSR J0837–2454 with the ATCA telescope. We detect the pulsar in our ATCA data and discovered low surface brightness diffuse emission surrounding the pulsar in archival GLEAM data. The low surface brightness diffuse emission, which if we assume to be the SNR, implies a low local free electron density in the pulsar environment, which is consistent with the prediction from the NE2001 model. Based on a geometrical analysis of a putative SNR identified at low frequencies, we derive a distance of ~0.9 kpc to the pulsar–SNR system. We also detect colocated H$\alpha$ emission from the SHASSA survey at the position of the pulsar. The morphology of this H$\alpha$ emission is inconsistent with the morphology of the GLEAM diffuse emission. Assuming that the excess DM comes from this H$\alpha$ complex, we estimate the distance to the pulsar to be ~0.2 kpc. Both of these distance estimates are significantly smaller than the predictions based on the NE2001 and YMW models, highlighting the uncertainty in estimating distances to pulsars using dispersion measures. The new distance estimates also result in z-heights for the pulsar, which are consistent with other pulsars of similar age.

The discrepancies in the distance estimates based on the electron density models and the geometric approach point to an important caveat relating to the identification of fast radio bursts (FRBs). The fundamental basis of "extragalactic" FRB identification relies on determining the Galactic contribution to the total DM observed for FRBs. The significant error in the leading electron densities toward the anticenter that are implied by our observations (factors of 10–20) indicate that care must be taken in the interpretation of transient discoveries (repeating and nonrepeating) as Galactic or extragalactic toward this region of the sky (Keane 2016).

However, if the NE2001-derived distance is accurate, then that, coupled with the young age of the pulsar, would imply that the pulsar was likely born close to its current observed position. This would imply that the progenitor O/B star would have to be a runaway star, making this the first pulsar known to be born from a runaway progenitor star.

## Appendix
## Point Sources Detected in ATCA Field of View

In Table 2, we list the point sources that were detected in the ATCA field of view along with their association to known point sources in the NVSS and SIMBAD catalog.

**Table 2**
The Point Sources Detected in the Uniform Weighted Image (Figure 3) Along with Their Association to Known Point Sources in the NVSS and SIMBAD Catalogs

| Sr. No. | Ident. | R.A. (hh:mm:ss.sss) | Decl. (dd:mm:ss.ss) | Integrated Flux (mJy) |
|---|---|---|---|---|
| 1 | NVSS 083817-251133 | $08:38:17.038 \pm 0.022$ s | $-25:11:40.028 \pm 0.142$ s | $37.60 \pm 2.300$ |
| 2. | NVSS 083732-244611 | $08:37:32.049 \pm 0.014$ s | $-24:46:16.948 \pm 0.087$ s | $16.57 \pm 0.630$ |
| 3. | NVSS 083839-245106 | $08:38:39.814 \pm 0.012$ s | $-24:51:09.144 \pm 0.076$ s | $14.77 \pm 0.460$ |
| 4. | NVSS 083814-245127 | $08:38:14.333 \pm 0.008$ s | $-24:51:28.966 \pm 0.057$ s | $8.960 \pm 0.200$ |
| 5. | NVSS 083801-245739 | $08:38:01.349 \pm 0.007$ s | $-24:57:42.372 \pm 0.043$ s | $5.049 \pm 0.093$ |
| 6. | NVSS 083746-245530 | $08:37:46.651 \pm 0.012$ s | $-24:55:33.085 \pm 0.076$ s | $4.190 \pm 0.130$ |
| 7. | NVSS 083853-244609 | $08:38:54.054 \pm 0.050$ s | $-24:46:17.975 \pm 0.210$ s | $3.170 \pm 0.290$ |
| 8. | NVSS 083751-244811 | $08:37:52.272 \pm 0.025$ s | $-24:48:13.889 \pm 0.132$ s | $2.840 \pm 0.170$ |
| 9. | NVSS 083654-244656 | $08:36:54.079 \pm 0.082$ s | $-24:46:53.655 \pm 0.418$ s | $2.700 \pm 0.640$ |
| 10. | NVSS 083648-245309 | $08:36:48.320 \pm 0.021$ s | $-24:53:16.525 \pm 0.247$ s | $0.965 \pm 0.140$ |
| 11. | ⋯ | $08:38:53.226 \pm 0.023$ s | $-24:58:45.749 \pm 0.254$ s | $0.894 \pm 0.101$ |
| 12. | NVSS 083713-245111 | $08:37:13.842 \pm 0.043$ s | $-24:51:12.270 \pm 0.326$ s | $0.774 \pm 0.114$ |
| 13. | ⋯ | $08:37:51.795 \pm 0.051$ s | $-24:58:51.020 \pm 0.327$ s | $0.494 \pm 0.079$ |
| 14. | ⋯ | $08:37:41.857 \pm 0.039$ s | $-24:51:36.157 \pm 0.236$ s | $0.444 \pm 0.049$ |
| 15. | ⋯ | $08:38:00.101 \pm 0.057$ s | $-24:51:54.951 \pm 0.364$ s | $0.431 \pm 0.069$ |
| 16. | ⋯ | $08:37:49.562 \pm 0.041$ s | $-24:50:32.491 \pm 0.243$ s | $0.343 \pm 0.048$ |
| 17. | ⋯ | $08:37:48.019 \pm 0.074$ s | $-24:56:57.376 \pm 0.451$ s | $0.311 \pm 0.059$ |
| 18. | ⋯ | $08:37:23.562 \pm 0.008$ s | $-24:48:04.798 \pm 0.161$ s | $0.305 \pm 0.034$ |
| **19.** | **PSR J0837–2454** | $\mathbf{08:37:57.723 \pm 0.086}$ **s** | $\mathbf{-24:54:27.599 \pm 0.571}$ **s** | $\mathbf{0.174 \pm 0.048}$ |

**Note.** In the case where the source had been identified in both catalogs, we list the identification associated with the NVSS catalog.

## ORCID iDs

Sarah Burke-Spolaor ⓘ https://orcid.org/0000-0003-4052-7838
Natasha Hurley-Walker ⓘ https://orcid.org/0000-0002-5119-4808
Harsha Blumer ⓘ https://orcid.org/0000-0003-4046-884X
Simon Johnston ⓘ https://orcid.org/0000-0002-7122-4963
Evan F. Keane ⓘ https://orcid.org/0000-0002-4553-655X
Marta Burgay ⓘ https://orcid.org/0000-0002-8265-4344
Andrea Possenti ⓘ https://orcid.org/0000-0001-5902-3731
N. D. Ramesh Bhat ⓘ https://orcid.org/0000-0002-8383-5059

## References

Abdo, A. A., Ackermann, M., Atwood, W. B., et al. 2008, Sci, 322, 1218
Acero, F., Ackermann, M., Ajello, M., et al. 2015, ApJS, 218, 23
Alsabti, A. W., & Murdin, P. 2017, Handbook of Supernovae (Berlin: Springer)
Arzoumanian, Z., Chernoff, D. F., & Cordes, J. M. 2002, ApJ, 568, 289
Atwood, W. B., Abdo, A. A., Ackermann, M., et al. 2009, ApJ, 697, 1071
Bannister, K. W., & Madsen, G. J. 2014, MNRAS, 440, 353
Bell, A. R. 1978, MNRAS, 182, 147
Blandford, R. D., & Ostriker, J. P. 1978, ApJL, 221, L29
Boch, T., & Fernique, P. 2014, in ASP Conf. Ser., 485, Astronomical Data Analysis Software and Systems XXIII, ed. N. Manset & P. Forshay (San Francisco, CA: ASP), 277
Bonnarel, F., Fernique, P., Bienaymé, O., et al. 2000, A&AS, 143, 33
Brazier, K. T. S., & Johnston, S. 1999, MNRAS, 305, 671
Briggs, D. S. 1995, AAS, 27, 1444
Burke-Spolaor, S., Bailes, M., Johnston, S., et al. 2011, MNRAS, 416, 2465
Camilo, F., Manchester, R. N., Gaensler, B. M., Lorimer, D. R., & Sarkissian, J. 2002, ApJL, 567, L71
Camilo, F., Ransom, S. M., Gaensler, B. M., et al. 2006, ApJ, 637, 456
Chatterjee, S., Brisken, W. F., Vlemmings, W. H. T., et al. 2009, ApJ, 698, 250
Cioffi, D. F., McKee, C. F., & Bertschinger, E. 1988, ApJ, 334, 252
Coles, W., Hobbs, G., Champion, D. J., Manchester, R. N., & Verbiest, J. P. W. 2011, MNRAS, 418, 561
Condon, J. J., Cotton, W. D., Greisen, E. W., et al. 1998, AJ, 115, 1693
Cordes, J. M., & Lazio, T. J. W. 2002, arXiv astrophysics
Deller, A. T., Goss, W. M., Brisken, W. F., et al. 2019, ApJ, 875, 100
Deller, A. T., Tingay, S. J., Bailes, M., & Reynolds, J. E. 2009, ApJ, 701, 1243
Espinoza, C. M., Lyne, A. G., Kramer, M., Manchester, R. N., & Kaspi, V. M. 2011, ApJL, 741, L13
Ferris, R. H., & Saunders, S. J. 2004, ExA, 17, 269
Frail, D. A., Giacani, E. B., Goss, W. M., & Dubner, G. 1996, ApJL, 464, L165
Frail, D. A., Goss, W. M., & Whiteoak, J. B. Z. 1994, ApJ, 437, 781
Gaensler, B. M., Madsen, G. J., Chatterjee, S., & Mao, S. A. 2008, PASA, 25, 184

Gaustad, J. E., McCullough, P. R., Rosing, W., & Van Buren, D. 2001, PASP, 113, 1326
Gotthelf, E. V., & Halpern, J. P. 2007, ApJL, 664, L35
Green, D. A. 1984, MNRAS, 209, 449
Green, D. A. 2019, JApA, 40, 36
Hills, J. G. 1983, ApJ, 267, 322
Hoffer, J. B. 1983, AJ, 88, 1420
Hotan, A. W., van Straten, W., & Manchester, R. N. 2004, PASA, 21, 302
Humason, M. L., & Zwicky, F. 1947, ApJ, 105, 85
Hurley-Walker, N., Callingham, J. R., Hancock, P. J., et al. 2017, MNRAS, 464, 1146
Hut, P., & Bahcall, J. N. 1983, ApJ, 268, 319
Igoshev, A. P. 2020, MNRAS, 494, 3663
Intema, H. T., Jagannathan, P., Mooley, K. P., & Frail, D. A. 2017, A&A, 598, A78
Kaspi, V. M., Roberts, M. E., Vasisht, G., et al. 2001, ApJ, 560, 371
Keane, E. F. 2016, MNRAS, 459, 1360
Keith, M. J., Jameson, A., van Straten, W., et al. 2010, MNRAS, 409, 619
Kramer, M., Lyne, A. G., Hobbs, G., et al. 2003, ApJL, 593, L31
Kulkarni, S. R., Ofek, E. O., Neill, J. D., Zheng, Z., & Juric, M. 2014, ApJ, 797, 70
Lorimer, D. R., & Kramer, M. 2012, Handbook of Pulsar Astronomy (Cambridge: Cambridge Univ. Press)
Lyne, A. G., Pritchard, R. S., Graham-Smith, F., & Camilo, F. 1996, Natur, 381, 497
Maíz-Apellániz, J. 2001, AJ, 121, 2737
McLaughlin, M. A., Arzoumanian, Z., Cordes, J. M., et al. 2002, ApJ, 564, 333
McMullin, J. P., Waters, B., Schiebel, D., Young, W., & Golap, K. 2007, in ASP Conf. Ser., 376, Astronomical Data Analysis Software and Systems XVI, ed. R. A. Shaw, F. Hill, & D. J. Bell (San Francisco, CA: ASP), 127
Migliazzo, J. M., Gaensler, B. M., Backer, D. C., et al. 2002, ApJ, 567, L141
Noutsos, A., Schnitzeler, D. H. F. M., Keane, E. F., Kramer, M., & Johnston, S. 2013, MNRAS, 430, 2281
Price, D. C., Staveley-Smith, L., Bailes, M., et al. 2016, JAI, 5, 1641007
Renzo, M., Zapartas, E., de Mink, S. E., et al. 2019, A&A, 624, A66
Reynolds, S. P., Gaensler, B. M., & Bocchino, F. 2012, SSRv, 166, 231
Sana, H., de Mink, S. E., de Koter, A., et al. 2012, Sci, 337, 444
Schure, K. M., Bell, A. R., O'C Drury, L., & Bykov, A. M. 2012, SSRv, 173, 491
Sedov, L. I. 1959, Similarity and Dimensional Methods in Mechanics (New York: Academic)
Shannon, R. M., & Cordes, J. M. 2010, ApJ, 725, 1607
Shklovskii, I. S. 1970, SvA, 13, 562
Sun, X.-H., & Reich, W. 2010, RAA, 10, 1287
van Straten, W., & Bailes, M. 2011, PASA, 28, 1
Wenger, M., Ochsenbein, F., Egret, D., et al. 2000, A&AS, 143, 9
Wolszczan, A., Cordes, J. M., & Dewey, R. J. 1991, ApJL, 372, L99
Yao, J. M., Manchester, R. N., & Wang, N. 2017, ApJ, 835, 29
Zeiger, B. R., Brisken, W. F., Chatterjee, S., & Goss, W. M. 2008, ApJ, 674, 271